Indications for the Substantial Predominance of Short-Range Effects on Inelastic Coulomb Form Factors for Various States in the ^{26}Mg Nucleus

Altaf A. Al-Rahmani[1]*, Sanna N. Fadhil[1], Adel K. Hamoudi[2]

[1]*Department of Physics, College of Science for Women, University of Baghdad, Baghdad, Iraq*
[2]*Department of Optics Techniques, Al-Farabi University College, Baghdad, Iraq*

Abstract

Short-range effects on C2, C3, as well as C4 form factors in the ^{26}Mg nucleus, were examined. The charge density distribution in this nucleus was also tested by means of one and two body fragments of cluster enlargement in cooperation with single-particle wave functions of harmonic potential. The correlation of Jastrow form was employed to inset the influence of short-range into the two body fragment of cluster enlargement. The nucleus of ^{26}Mg was assumed to own a ^{16}O-core with (A-16) nucleons dispersed over the sd-model space. The form factors in ^{26}Mg nucleus ascend from the core-polarization and model space involvements. The form of Tassie model, subject to the charge density, was used to determine the transition density of core polarization. The one body density matrix elements required for determining the transition density of model space for various transitions in ^{26}Mg were found via carrying out shell model computations using the OXBASH program with the universal-sd interaction of Wildenthal. The present calculations were subjected to the oscillator and correlation parameters symbolized by b and β, respectively. These parameters are self-sufficiently generated for every specific nucleus by fitting between the calculated and observed elastic form factors. For determining the charge density, elastic form factors and inelastic Coulomb form factors for dissimilar excited states in ^{26}Mg, one value is needed for b and β. This study shows indications for the substantial predominance of short-range influences on current computations, where considering these influences look to be requisite for carrying out a distinguished adjustment in calculated results which ultimately leads to a remarkable explication of the data throughout all the considered momentum transfers.

Keywords: Electron scattering; Elastic form factors; Inelastic form factors; Charge density; Short range correlation; sd-shell model; ^{26}Mg nucleus

مؤشرات مهمة لهيمنة تأثيرات المدى القصير على عوامل التشكل الكولومية غير المرنة لحالات مختلفة في نواة المغنيسيوم-26

الطاف عبد المجيد الرحماني^{1}*، سناء نجاح فاضل^{1}، عادل خلف حمودي^{2}

^{1}قسم الفيزياء، كلية العلوم للبنات، جامعة بغداد، بغداد، العراق
^{2}قسم التقنيات البصرية، كلية الفارابي الجامعة، بغداد، العراق

---
*Email: altafha_phys@csw.uobaghdad.edu.iq

الخلاصة

تم اختبار تأثيرات المدى القصير على عوامل التشكل الكولومي C2، C3 و C4 الغير مرن في نواة المغنيسيوم–26. وتم أيضًا اختبار كثافة الشحنة لهذه النواة من خلال استخدام حد الجسيم المنفرد وحد الجسيمتين من امتداد كلاستر (Cluster enlargement) وبالتعاون مع دوال موجة الجسيم المنفرد للجهد التوافقي. تم استخدام دالة ارتباط صيغة جاسترو (Jastrow form) لأدخال تأثير المدى القصير في حد الجسيمتين من امتداد كلاستر. هنا أُفترضنا بأن نواة المغنيسيوم–26 تتألف من قلب مغلق هو الأوكسجين–16 مع (A–16) جسيمة موزعة على أنموذج الفضاء sd. ان عوامل التشكل في نواة المغنيسيوم–26 تنشأ من مساهمتين هما استقطاب اللقلب وأنموذج الفضاء. هنا استخدامنا أنموذج تاسي (Tassie model)، الذي يعتمد على كثافة الشحنة، لأيجاد كثافة أنتقال شحنة أستقطاب القلب. وجدنا عناصر مصفوفة كثافة الجسم المنفرد (OBDM)، اللازمة في حساب كثافة انتقال شحنة انموذج الفضاء، ولأنتقالات مختلفة في نواة المغنيسيوم–26 من خلال اجراء حسابات أنموذج القشرة النووية بواسطة البرنامج الحاسوبي OXBAH سوية مع تفاعل والدنثال العام للقشرة sd (.universal–sd interaction of Wildenthal). تعتمد الحسابات الحالية على معلمة حجم المتذبذب b ومعلمة الأرتباط β. وجدنا قيم المعلمتين b و β عن طريق ملاءمة عوامل التشكل المرنة المحسوبة لنواة المغنيسيوم–26 مع النتائج العملية. لغرض تحديد كثافة الشحنة، عوامل التشكل المرنة وعوامل التشكل الغير المرنة لحالات متهيجة مختلفة في نواة المغنيسيوم–26، نحتاج قيمة واحدة فقط لكل من b و β. تُظهر هذه الدراسة مؤشرات مهمة لهيمنة تأثيرات المدى القصير على الحسابات الحالية، حيث يبدو أن النظر في هذه التأثيرات ضروري لإجراء تعديل مميز في النتائج المحسوبة مما يؤدي في النهاية إلى تفسير البيانات بشكل ملحوظ على طول الزخم المنتقل قيد الدراسة.

1. Introduction

The most complex system in nature is the nucleus. The main task in exemplifying nuclei is to comprehend the short inter-particle segment of nuclear wave functions. The task is a result of the complex interactions among nucleons and the substantial nuclear density. Moreover, it ensures that all essential measurements of the nucleus (for instance, the nucleon size, the interaction range and the mean distance) to be good, making actual theoretical descriptions rather difficult [1]. In addition, comprehensive information of Short-Range Correlations (SRC's) is fundamental to the structure of neutron and the nuclear symmetry energy [2, 3], the bound nucleon and the structure functions of free neutron [4–8], as well as the neutrino oscillation investigations and neutrino-nucleus interactions [9–13].

Various nuclear static properties are adequately clarified by existing models of average field [14, 15], but not go as planned to elucidate the influence of SRC's dynamic. Ab-initio reckonings of many nucleon schemes [16–19] are still constrained to light nuclei as well as soft interactions which modify short-range components in nuclear wave function. As a result, real models are still desired to categorize the main physical technique at short distances and to elucidate the mid and high mass nuclei [20–22].

The insert of SRC's into the Slater determinant were achieved by by Massen et al. [23], Massen and Panos [24], and Massen [25], joining commonly the $N = Z$ light nuclei from the standpoint of Born approach. Clark and Ristig [26], Ristig et al. [27], and Clark [28] utilized the factor cluster expansion in an effort to create a formula for elastic form factors $F_{el}(q)$, shortened at two body fragments. This formula of $F_{el}(q)$ was used in closed (^{4}He, ^{16}O and ^{40}Ca) nuclei and open s-, p-, as well as sd-nuclei. The SRC's influences on s, p, and sd nuclei were accomplished by Massen and Moustakidis [29] precisely departing from the method used by Massen et al. [23], Massen and Panos [24], and Massen [25]. Jastrow [30] used the cluster enlargement and Jastrow function that interpolate SRC's, to imitate explicit formulas

to densities $\rho(r)$ and $F_{el}(q)$. Actually, these formulas rely on the motion of a single particle [31-33] rather than the relative 2-particle wave functions [22, 34]. It is crucial to assert that the aforementioned investigations were only focused on effects of SRC's on $F_{el}(q)$.

Inelastic coulomb form factors $[F_{inel.}(q)]$ with the attachment of SRC's in $^{58-64}$N-nuclei have recently been examined by Abbas and Hamoudi [35]. These nuclei comprise a ^{56}Ni-core and (A-56) neutrons distributed over f5p space (defined by 1f$_{5/2}$, 2p$_{3/2}$ and 2p$_{1/2}$ orbitals). Indeed, because active protons are absent from the f5p-space, the calculated results of Abbas and Hamoudi [35] were due only to the core-polarization involvement.

In the current research, the influences of SRC's on $F_{inel}(q)$ in ^{26}Mg nucleus was inspected, where the calculated results arise from the contributions of the core-polarization and model space. The research showed that there is a signal for the considerable predominance of short range influences on the current computations, where implantation of SRC's on $F_{inel}(q)$ looks to be essential to obtain a noticeable improvement in the calculated results, which eventually leads to interpret the data astonishingly over the momentum transfer under consideration.

2. Theory

The inelastic form factor in electron-nucleus scattering is specified by the following equation [36]:

$$\left| F_J^L(q) \right|^2 = \frac{4\pi}{Z^2(2J_i+1)} \left| \left\langle f \left\| \hat{T}_J^L(q) \right\| i \right\rangle \right|^2 \left| F_{cm}(q) \right|^2 \left| F_{fs}(q) \right|^2, \tag{1}$$

Where the momentum transfer and angular momentum are indicated by q and J, respectively, the initial $\left| i \right\rangle = \left| J_i T_i \right\rangle$ and final $\left| f \right\rangle = \left| J_f T_f \right\rangle$ states are described by $J_{i/f}$ (spin) and $T_{i/f}$ (isospin), the electron-nucleus scattering Coulomb operator is represented by $\hat{T}_J^L(q)$, the center of mass correction is symbolized by $F_{cm}(q) = e^{q^2 b^2 / 4A}$ (which is accountable for disregarding false states formed from the center of mass motion as soon as the shell model wave function is employed), the finite-sized nucleon correction is depicted by $F_{fs}(q) = e^{-0.43q^2/4}$ (which is assumed to be analogous for protons and neutrons), the atomic and mass numbers are denoted by Z and A, respectively, and the parameter b is defined by $b = \sqrt{\hbar/(M_p \omega)}$ [37], where $\hbar = h/2\pi$ (h is Plank's constant) while ω and M_p are the angular frequency and the proton mass, respectively. Abridging the matrix element presented in Eq. (1) in spin and isospin, Eq. (1) changes to [38]:

$$\left| F_J^L(q) \right|^2 = \frac{4\pi}{Z^2(2J_i+1)} \left| \sum_{T=0,1} (-1)^{T_f - T_{z_f}} \begin{pmatrix} T_f & T & T_i \\ -T_{z_f} & 0 & T_{z_i} \end{pmatrix} \left\langle J_f T_f \left\| \hat{T}_{JT}^L(q) \right\| J_i T_i \right\rangle \right|^2$$

$$\times \left| F_{cm}(q) \right|^2 \left| F_{fs}(q) \right|^2. \tag{2}$$

In Eq. (2), the 3-J symbol is represented by the bracket while the isospin T and isospin projection T_Z are demarcated as:

$$\left| T_f - T_i \right| \leq T \leq T_f + T_i, \text{ and } T_Z = \frac{Z-N}{2}. \tag{3}$$

The abridged matrix, displayed in Eq. (2), amid the states $\left| i \right\rangle$ and $\left| f \right\rangle$ of many-body scheme is given via multiplying the One-Body Density Matrix (OBDM) and single-particle matrix elements of Coulomb operator [37]:

$$\left\langle f \left\| \hat{T}_{JT}^{L} \right\| i \right\rangle = \sum_{a,b} OBDM^{JT}(i,f,J,a,b) \left\langle b \left\| \hat{T}_{JT}^{L} \right\| a \right\rangle, \tag{4}$$

Where the states of a single-particle are signified by the symbols a and b. The OBDM, shown in Eq. (4), is evaluated by [39]:

$$OBDM(\tau_z) = (-1)^{T_f - T_z} \begin{pmatrix} T_f & 0 & T_i \\ -T_z & 0 & T_z \end{pmatrix} \sqrt{2} \frac{OBDM(\Delta T = 0)}{2}$$

$$+ \tau_z (-1)^{T_f - T_z} \begin{pmatrix} T_f & 1 & T_i \\ -T_z & 0 & T_z \end{pmatrix} \sqrt{6} \frac{OBDM(\Delta T = 1)}{2}, \tag{5}$$

Where the single-particle isospin operator is represented by τ_z.

To create the abridged matrix of many-body scheme of $\hat{T}_J^L(q)$ operator, the core polarization (cp) and model space (ms) involvements are added [39]:

$$\left\langle f \left\| \hat{T}_J^L(\tau_z, q) \right\| i \right\rangle = \left\langle f \left\| \hat{T}_J^{L\,ms}(\tau_z, q) \right\| i \right\rangle + \left\langle f \left\| \hat{T}_J^{L\,cp}(\tau_z, q) \right\| i \right\rangle. \tag{6}$$

The ms involvement is expressed by:

$$\left\langle f \left\| \hat{T}_J^{L\,ms}(\tau_z, q) \right\| i \right\rangle = \int_0^\infty dr\, r^2\, j_J(qr)\, \rho_{J,\tau_z}^{ms}(i,f,r), \tag{7}$$

Where the spherical Bessel function is symbolized by $j_J(qr)$, and the transition charge density of ms is symbolized by $\rho_{J,\tau_z}^{ms}(i,f,r)$ and given by [39]:

$$\rho_{J,\tau_z}^{ms}(i,f,r) = \sum_{jj'(ms)}^{ms} OBDM(i,f,J,j,j',\tau_z) \left\langle j \| Y_J \| j' \right\rangle R_{nl}(r)\, R_{n'l'}(r), \tag{8}$$

Where the radial and spherical parts of the harmonic oscillator wave function are denoted by $R_{nl}(r)$ and Y_J, respectively.

The cp involvement is expressed by:

$$\left\langle f \left\| \hat{T}_J^{L\,cp}(\tau_z, q) \right\| i \right\rangle = \int_0^\infty dr\, r^2\, j_J(qr)\, \rho_{J,\tau_z}^{cp}(i,f,r), \tag{9}$$

Where the transition charge density of cp, denoted by $\rho_{J\tau_z}^{cp}(i,f,r)$, is reliant on the form utilized for cp. The nuclear collective behaviors $\rho_{J,\tau_z}^{ms}(i,f,r)$ ought to be supplementary to $\rho_{J\tau_z}^{cp}(i,f,r)$. Thus a complete transition density takes the form:

$$\rho_{J\tau_z}(i,f,r) = \rho_{J\tau_z}^{ms}(i,f,r) + \rho_{J\tau_z}^{cp}(i,f,r) \tag{10}$$

In cooperation with the nuclear collective behaviors, the $\rho_{J\tau_z}^{cp}(i,f,r)$ is anticipated to own the form of Tassie shape [40]:

$$\rho_{J t_z}^{cp}(i,f,r) = N_T \frac{1}{2}(1 + \tau_z) r^{J-1} \frac{d\rho_{ch}^{gs}(i,f,r)}{dr}, \tag{11}$$

Where

$$N_T = \frac{\int_0^\infty dr\, r^{J+2} \rho_{t_z}^{ms}(i,f,r) - \sqrt{(2J_i + 1) B(CJ)}}{(2J+1)\int_0^\infty dr\, r^{2J} \rho_{ch}^{gs}(i,f,r)}, \tag{12}$$

denotes the normalization constant obtained via amending of the reduced probability $B(CJ)$ to the observed one, and $\rho_{ch}^{gs}(i, f, r)$ denotes the nuclear charge density of ground state.

For closed shell nuclei with $N = Z$, the $\rho_{ch}^{gs}(r)$ is related to the ground state point nucleon density $\rho_p^{gs}(r)$ by:

$$\rho_{ch}^{gs}(r) = \frac{1}{2}\rho_p^{gs}(r), \qquad \text{(in e.fm}^{-3}\text{)} \tag{13}$$

To add in the influence of SRC's into $\rho_p^{gs}(r)$, the nuclear wave functions are formulated by:

$$\Psi = F\,\Phi, \tag{14}$$

Where: F represents a model operator that inserts SRC's and Φ represents the wave function of a Slater determinant. The operator F must be symmetric in its argument $(1\ldots i\ldots A)$, translationally invariant, and possesses the cluster condition. To be more precise, when a nucleon subdivision $(i_1\ldots i_p)$ is separated from the remaining $(i_{p+1}\ldots i_A)$, F disconnects into a combination of two variables, $F(1\ldots A) = F(i_1\ldots i_p)\,F(i_{p+1}\ldots i_A)$ [28]. In the current investigation, F is assumed as a Jastrow type [30]:

$$F = \prod_{i<j}^{A} f(r_{ij}), \tag{15}$$

Where the two particles SRC's, $f(r_{ij}) = f(\left|\vec{r}_i - \vec{r}_j\right|)$, are a function of a state sovereign given by: $f(r_{ij}) = 1 - \exp[-\beta(\vec{r}_i - \vec{r}_j)^2], \tag{16}$

and possesses the attributes: $f(r_{ij}) \to 1$ for enormous magnitudes of $\vec{r}_{ij} = \left|\vec{r}_i - \vec{r}_j\right|$ and $f(r_{ij}) \to 0$ for $\vec{r}_{ij} \to 0$. As a result, the SRCs influences implanted by Eq. (16) comes to be substantial for the slight magnitudes of β and vice versa.

The formulation of $\rho_p^{gs}(r)$ is given by [29]:

$$\rho_p^{gs}(r) = N_D\left\langle \Psi(\vec{r}_1, \vec{r}_2,...,\vec{r}_A)\left|\hat{O}_r\right|\Psi(\vec{r}_1, \vec{r}_2,...,\vec{r}_A)\right\rangle$$
$$= N_D\left\langle \hat{O}_r \right\rangle. \tag{17}$$

Here $\Psi(\vec{r}_1, \vec{r}_2,...,\vec{r}_A)$ signifies the nuclear wave function shown in Eq. (14), $N_D = \left\langle \Psi(\vec{r}_1, \vec{r}_2,...,\vec{r}_A)\left|\Psi(\vec{r}_1, \vec{r}_2,...,\vec{r}_A)\right\rangle\right.^{-1}$ denotes the normalization factor that is determined by $4\pi\int_0^\infty \rho_p^{gs}(r)\,r^2 dr = 1$, and $\hat{O}_r$ symbolizes the 1-body density operator formulated as

$$\hat{O}_r = \sum_{i=1}^{A}\hat{o}_r(i) = \sum_{i=1}^{A}\delta(\vec{r} - \vec{r}_i). \tag{18}$$

To determine the distribution of $\rho_p^{gs}(r)$, the generalized normalization integral was used[29]:

$$I(\alpha) = \left\langle \Psi\left|[\exp[\alpha\,I(0)\,\hat{O}_r\right|\Psi\right\rangle, \tag{19}$$

analogous to the operator $\hat{O}_r$ from:

$$\left\langle \hat{O}_r \right\rangle = \left[\frac{\partial \ln I(\alpha)}{\partial \alpha}\right]_{\alpha=0}. \tag{20}$$

In cluster study of Eq. (20), the integrals $I_i(\alpha)$, $I_{ij}(\alpha)$ ... were used for subdivisions of a system which possesses A nucleons and a factor cluster deconstruction of these integrals. The expectation value of $\hat{O}_r$ is expressed as [29]:

$$\rho_p^{gs}(r) = N_D \langle \hat{O}_r \rangle = N_D \left\{ \langle \hat{O}_r \rangle_1 + \langle \hat{O}_r \rangle_2 + ... + \langle \hat{O}_r \rangle_A \right\}, \tag{21}$$

Where [29]:

$$\langle \hat{O}_r \rangle_1 = \sum_{i=1}^{A} \left[\frac{\partial \ln I_i(\alpha)}{\partial \alpha} \right]_{\alpha=0} = \sum_{i=1}^{A} \langle i | F_1^+ \hat{o}_r(1) F_1 | i \rangle, \tag{22}$$

$$\langle \hat{O}_r \rangle_2 = \sum_{i<j}^{A} \frac{\partial}{\partial \alpha} \left[\ln I_{ij}(\alpha) - \ln I_i(\alpha) - \ln I_j(\alpha) \right]_{\alpha=0}$$
$$= \sum_{i<j}^{A} \langle ij | F_{12}^+ [\hat{o}_r(1) + \hat{o}_r(2)] F_{12} | ij \rangle_a - \sum_{i<j}^{A} \left[\langle i | \hat{o}_r(1) | i \rangle + \langle j | \hat{o}_r(2) | j \rangle \right], \tag{23}$$

and so on. Hence, the identity operator is assumed to be F_1.

The cluster expansion causes to breakup of 1-body, 2-body, ..., A-body correlation effects on the density. Here, three-body and many-body components would not be used in this study. As a result, the correlated density $\rho_p^{gs}(r)$ of Eq. (21) (whch includes the influence of SRC's) converts into:

$$\rho_p^{gs}(r) \approx N_D \left\{ \langle \hat{O}_r \rangle_1 + \langle \hat{O}_r \rangle_2 \right\}. \tag{24}$$

Applying Eqs. (22) and (23) to Eq. (24), we get:

$$\rho_p^{gs}(r) \approx N_D \left\{ \sum_{i=1}^{A} \langle i | \hat{o}_r(1) | i \rangle + 2 \sum_{i<j}^{A} \langle ij | F_{12}^+ \hat{o}_r(1) F_{12} | ij \rangle_a - 2 \sum_{i<j}^{A} \langle ij | \hat{o}_r(1) | ij \rangle_a \right\}. \tag{25}$$

For simplicity, Eq. (25) is expressed in a dissimilar formula as:

$$\rho_p^{gs}(r) \approx N_D \left\{ \langle \hat{O}_r \rangle_1 + \langle \hat{O}_r \rangle_{22} - \langle \hat{O}_r \rangle_{21} \right\} \tag{26}$$

where

$$\langle \hat{O}_r \rangle_1 = \sum_{i=1}^{A} \langle i | \hat{o}_r(1) | i \rangle, \tag{27}$$

$$\langle \hat{O}_r \rangle_{22} = 2 \sum_{i<j}^{A} \langle ij | F_{12}^+ \hat{o}_r(1) F_{12} | ij \rangle_a, \tag{28}$$

$$\langle \hat{O}_r \rangle_{21} = 2 \sum_{i<j}^{A} \langle ij | \hat{o}_r(1) | ij \rangle_a \tag{29}$$

If the 2-particle correlation displayed in Eq. (16) is considered, then:

$$F_{12} F_{12} = \left(1 - \exp[-\beta(\vec{r}_1 - \vec{r}_2)^2]\right)\left(1 - \exp[-\beta(\vec{r}_1 - \vec{r}_2)^2]\right)$$
$$= 1 - 2g(r_1, r_2, \beta) + g(r_1, r_2, 2\beta) \tag{30}$$

Where:

$$g(r_1, r_2, z) = \exp(-z\, r_1^2) \exp(-z\, r_2^2) \exp(2\, z\, r_1\, r_2 \cos w_{12}), \quad (with\ z = \beta\ or\ 2\beta). \tag{31}$$

With the assistance of Eqs. (30) and (31), Eq. (28) converts to:

$$\langle \hat{O}_r \rangle_{22} = 2 \sum_{i<j}^{A} \langle ij | \hat{o}_r(1) \left[1 - 2g(r_1, r_2, \beta) + g(r_1, r_2, 2\beta) \right] | ij \rangle_a$$
$$= 2 \left\{ \sum_{i<j}^{A} \langle ij | \hat{o}_r(1) | ij \rangle_a - 2 \sum_{i<j}^{A} \langle ij | \hat{o}_r(1)\, g(r_1, r_2, \beta) | ij \rangle_a + \sum_{i<j}^{A} \langle ij | \hat{o}_r(1)\, g(r_1, r_2, 2\beta) | ij \rangle_a \right\} \tag{32}$$

For simplicity, Eq. (32) may be formulated as:

$$\left\langle \hat{O}_r \right\rangle_{22} = \left\langle \hat{O}_r \right\rangle_{21} - 2O_{22}(r,\beta) + O_{22}(r,2\beta) \tag{33}$$

Where the 2- particle part $O_{22}(r,z)$ is expressed as:

$$O_{22}(r,z) = 2\sum_{i<j}^{A} \left\langle ij \middle| \hat{o}_r(1)\, g(r_1,r_2,z) \middle| ij \right\rangle_a . \tag{34}$$

Utilizing Eq. (33) into Eq. (26), we get:

$$\rho_p^{gs}(r) \approx N_D \left\{ \left\langle \hat{O}_r \right\rangle_1 - 2O_{22}(r,\beta) + O_{22}(r,2\beta) \right\}, \tag{35}$$

Where $\rho_p^{gs}(r)$ is reliant on β inserted by the correlation of Jastrow-type.

The 1-particle component $\left\langle \hat{O}_r \right\rangle_1$, revealed in Eq. (35), is clearly specified and given by:

$$\begin{aligned} \left\langle \hat{O}_r \right\rangle_1 &= \sum_{i=1}^{A} \left\langle i \middle| \hat{o}_r(1) \middle| i \right\rangle \\ &= 4\sum_{nl} \eta_{nl}(2l+1)\frac{1}{4\pi}\phi_{nl}^*(r)\phi_{nl}(r), \end{aligned} \tag{36}$$

Where η_{nl} and $\phi_{nl}(r)$ symbolize the single particle's radial wave function and the occupation probability of the state nl, respectively. By means of the algebra of spherical harmonics, the formula of $O_{22}(r,z)$ exhibited in Eq. (34) changes to [29]:

$$\begin{aligned} O_{22}(r,z) = 4 \sum_{n_i l_i, n_j l_j} &\eta_{n_i l_i}\eta_{n_j l_j}(2l_i+1)(2l_j+1) \\ &\times \left\{ 4A_{n_i l_i n_j l_j}^{n_j l_j n_i l_i 0}(r,z) - \sum_{k=0}^{l_i+l_j}\left\langle l_i 0 l_j 0 \middle| k0 \right\rangle^2 A_{n_i l_i n_j l_j}^{n_j l_j n_i l_i k}(r,z) \right\}, \quad (z=\beta,\,2\beta) \end{aligned} \tag{37}$$

where

$$\begin{aligned} A_{n_1 l_1 n_2 l_2}^{n_3 l_3 n_4 l_4 k}(r,z) = &\frac{1}{4\pi}\phi_{n_1 l_1}^*(r)\phi_{n_3 l_3}(r)\exp(-zr^2) \\ &\times \int_0^\infty \phi_{n_2 l_2}^*(r_2)\phi_{n_4 l_4}(r_2)\exp(-zr_2^2)\, i_k(2zrr_2)r_2^2\, dr_2 , \end{aligned} \tag{38}$$

with $\left\langle l_i 0 l_j 0 \middle| k0 \right\rangle$ and $i_k(x)$ stand for the coefficient of Clebsch Gordan and modified spherical Bessel function, respectively.

Actually, the formulae of Eqs. (13)-(38) are proposed for closed shell ($Z = N$) nuclei with $\eta_{nl} = 0$ or 1. For open shell ($Z \neq N$)1 nuclei, the same formulae can also be employed but with $0 \leq \eta_{nl} \leq 1$.

The definition of mean square charge radii is given by:

$$\left\langle r^2 \right\rangle = \frac{4\pi}{Z}\int_0^\infty \rho_{ch}^{gs}(r)\, r^4\, dr, \tag{39}$$

where

$$Z = 4\pi \int_0^\infty \rho_{ch}^{gs}(r)\, r^2\, dr, \tag{40}$$

is the normalization constant of $\rho_{ch}^{gs}(r)$.

Elastic electron scattering form factor $F_{el}(q)$ is associated with $\rho_{ch}^{gs}(r)$, where $F_{el}(q)$ is essentially the Fourier transform of $\rho_{ch}^{gs}(r)$. i.e.:

$$F_{el}(q) = \frac{4\pi}{Z} \int_0^\infty \rho_{ch}^{gs}(r) j_0(qr) r^2 dr \tag{41}$$

Including the corrections of center of mass $F_{cm}(q)$ and finite size $F_{fs}(q)$ into Eq. (41), we get:

$$F_{el}(q) = \frac{4\pi}{Z} \int_0^\infty \rho_{ch}^{gs}(r) j_0(qr) r^2 dr \, F_{cm}(q) F_{fs}(q) \tag{42}$$

3. Results and discussion

The computations of the charge density $\rho_{ch}^{gs}(r)$, elastic form factors $F_{el.}(q)$ and inelastic form factors $F_{inel.}(q)$ in ^{26}Mg nucleus were achieved. Two types of computations were executed employing harmonic wave functions of a single particle without (type-1) and with (type-2) comprising of SRCs. The computation of type-1 relies only on the parameter b but that of type-2 relies on the parameters b and β. The values of these parameters in type-1 {type-2}, presented in Table 1, were produced by revising b {b and β} in an attempt to imitate the measured rms radius $<r_{ch}^2>_{\exp.}^{1/2}$ {the $<r_{ch}^2>_{\exp.}^{1/2}$ and at the same time to fit the calculated $F_{el}(q)$ with those of measured ones}. The calculated rms radius $<r_{ch}^2>_{cal.}^{1/2}$ and the participation of SRCs, $<r^2>_2^{1/2} = \sqrt{<r_{ch}^2>_{cal.} - <r_{ch}^2>_1}$, to $<r_{ch}^2>_{cal.}^{1/2}$ in the nucleus under study are also presented in Table 1. The measured rms radius $<r_{ch}^2>_{\exp}^{1/2}$ [41, 42] of ^{26}Mg is also presented in the same Table for comparison. Actually, Table 1 demonstrates that b possesses the disparity relation: $b(\text{type-1}) > b(\text{type-2})$, where the inclusion of SRCs upsurges the relative distance amidst nucleons which serially induces an increase in nuclear size. Accordingly, the magnitude of b associated to the nuclear size (experimentally firm) requires to be abridged.

Table 1- Created values of b, β and the involvements of one particle and two particle densities to the complete rms charge radius [$<r_{ch}^2>_{Cal..}^{1/2}$ in ^{26}Mg nucleus. Type-1 indicates the computations of 1-body part (without SRCs) whereas type-2 indicates the computations of 1-body plus 2-body parts (with SRCs).

Type	b (fm)	β (fm^{-2})	rms charge radii [$<r_{ch}^2>_{Cal..}^{1/2}$] (fm)			$<r_{ch}^2>_{\exp.}^{1/2}$ (fm)
			Without SRC's (1-body part)	With SRC's (2-body part)	Total	
1	1.895	0	3.0938	0	3.0938	3.060 [41] 3.034 [42]
2	1.721	1.75	2.8103	1.1057	3.0200	

The computed $F_{el}(q)$ and $\rho_{ch}^{gs}(r)$ in ^{26}Mg nucleus are presented in Figure1(a) and Figure1(b), respectively.

In Figure 1(a), the elastic form factors are plotted against q. The blue and red solid curves stand for the calculated $F_{el}(q)$ without and with the attachment of SRCs effects, respectively. The open circle symbols stand for the experimental data of De Vries et al. [41], where the obtainable data for ^{26}Mg nucleus are restricted only on the momentum transfer region of $q \leq 1.15$ fm^{-1}. It is apparent that both computations of type-1 (blue solid curve) and type-2 (red solid curve) are in excellent accordance with the data. In fact, Figure 1(a) emphasizes that the SRCs have no effects on elastic form factors at momentum transfer region $q \leq 1.15$ fm^{-1} (where the blue and red solid curves coincided with each other) but beyond that region, the SRCs become operative on $F_{el}(q)$ (where these curves diverged noticeably from each other).

In Figure 1(b), the charge density $\rho_{ch}^{gs}(r)$ (in fm^{-3}) was plotted as a function of r (in fm). The open circle symbols signify the experimental charge density distribution [41] of ^{26}Mg nucleus whereas the blue and red solid curves signify the calculated $\rho_{ch}^{gs}(r)$ without and with the supplement of SRCs effects, respectively. The participation of SRCs $\rho_2(r) = \rho_{ch}^{gs}(r) - \rho_{1,ch}^{gs}(r)$ to $\rho_{ch}^{gs}(r)$ is also shown in Figure 1(b) by the red dashed curve, where the behavior of $\rho_2(r)$ is shown by downswing and upswing round the r-axis. It is so obvious that the central portion ($0 \leq r \leq 2$ fm^{-1}) {tail portion ($r > 2$ fm^{-1})} of open circle symbols distribution is noticeably under predicted {well predicted} by both computations of the blue and red solid curves. Also, the supplement of SRCs into the calculations of red solid curve makes a substantial reduction {an insubstantial increase} in the central portion {tail portion} of $\rho_{ch}^{gs}(r)$. This gives the interpretation that the supplement of SRCs causes to upsurge the opportunity of shifting the protons from the central part to the surface part of the nucleus which in turn causes to increase the rms charge radius of the nucleus. Hence, this leads to reduce the rigidity of the nucleus, which is in contrary to the situation of non-considering of the SRCs effects. To retain the nuclear size within the immobile measured results, the value of b was diminished when including the SRCs effects, see Table 1.
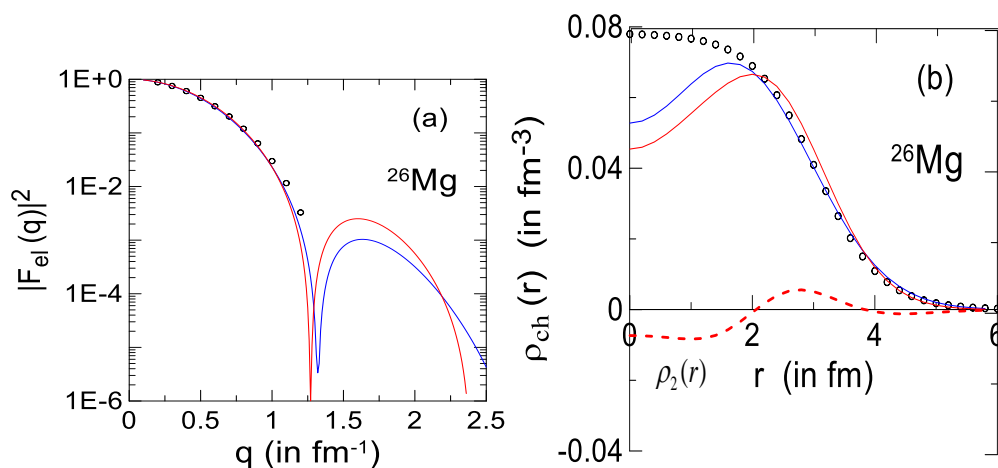
Figure 1: Elastic charge form factors $F_{el}(q)$ [Figure 1(a)] and the density distribution $\rho_{ch}^{gs}(r)$ [Figure 1(b)] in the ^{26}Mg nucleus. The blue and red solid curves are the obtained results without and with comprising the short range effects, respectively. The contribution of SRCs effects $\rho_2(r)$ to $\rho_{ch}^{gs}(r)$ is displayed in Figure 1(b) by the red dashed curve. The experimental data described by open circle symbols are taken from [41].

Next, the SRCs effects on inelastic form factors for different excited states in ^{26}Mg nucleus is discussed. This nucleus, which has a total isospin $T = 1$, is assumed to own a closed shell of ^{16}O-core and 10 valence nucleons (4 protons and 6 neutrons) distributed over the sd-shell model space defined by $1d_{5/2}$, $2s_{1/2}$ and $1d_{3/2}$ orbitals. The inelastic form factors in ^{26}Mg nucleus come up from both the cp transition charge density $\rho^{cp}_{J\tau_z}(i, f, r)$ and ms transition charge density $\rho^{ms}_{J\tau_z}(i, f, r)$. The cp effects on inelastic form factors were found by Tassie model (Eq. (11)) in cooperation with the computed $\rho^{gs}_{ch}(r)$. The USD interaction [43] was adopted to compute the OBDM elements of sd-space utilizing the OXBASH-code [44]. The form factors for different excited states in ^{26}Mg nucleus were computed using a single value for each b and β. These values (displayed in Table 1) were found by the fit to the experimental $F_{el}(q)$.

The comparison between the computed and measured inelastic Coulomb form factors for transitions ($J^{\pi}_{i=gs}T_i \rightarrow J^{\pi}_f T_f$) from the initial (ground) state 0^+1 to the final states 2^+1, 3^+1 and $4^+_f 1$ is displayed in Figs. 2 to 14, where all the transitions under study are of isovector character. The left and middle panels in these figures signify type-1 and type-2 computations obtained without and with the supplement of SRCs effects, respectively. The dashed curves stand for the participation of ms where the mixing of configurations is considered, the long-dashed curves stand for the participation of cp where the collective behaviors were taken into account and the solid curves stand for the complete participation obtained by adding the effects of ms and cp. To simplify the comparison, we display the total form factors of the blue solid curve (without SRCs) and red solid curve (with SRCs) in right panel.

The inelastic C2 form factors of $0^+1 \rightarrow 2^+1$ transitions are displayed in Figs. 2 to 7, where the parity of these transitions does not change between the initial and final states.

In Figure 2, the C2 outcomes for the 2^+1 state ($E_x = 1.809$ MeV with reduced transition probability B(C2) $= 275 \pm 20$ e^2.fm^4) [45] are displayed. The ms computation (blue dashed curve), which has the main participation in the left panel, is not enough to describe the measured form factors (open circles). It is obvious that the ms participation clearly under predicts the data at all momentum transfer under investigation. Considering the cp effect (blue long-dashed curve) as a supplement to the ms computation provides a substantial amendment to the C2 outcome. The influence of cp enhances the result (blue solid curve), where this curve (which is still under predicting the data) was closer to the data than that of the ms. In the middle panel of Figure 2, the computations were repeated exactly as in the left panel but this time the SRC's effect was comprised. In the right panel of Figure2, the comparison amongst the total C2 form factors without SRC's (blue solid curve) and with SRC's (red solid curve) together with those of the measured data (open circles) is displayed. It was noticed that the comprising of SRC's led to progress the outcomes (red solid curve) and made them in very good accordance with the data.
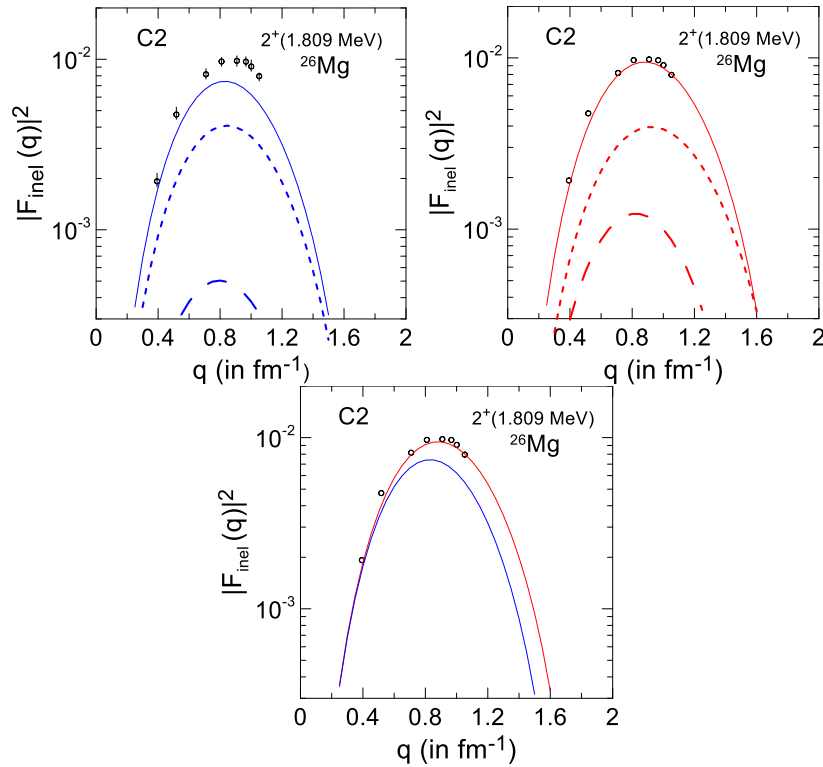
Figure 2: Square of inelastic form factors in ^{26}Mg nucleus for the state 2^+ (1.809 MeV). The left and middle panels are type-1 and type-2 calculations gotten without and with the supplement of SRC's effects, respectively. The dashed, long-dashed and solid curves are the ms, cp and total contributions, respectively. For comparison, the total form factors of the blue solid curve of the left panel (without SRC's effect) and the red solid curve of the middle panel (with SRCs effect) are displayed in the right panel. The experimental data (open circle symbols) are taken from [45].

In Figs. 3 to 7, the calculations are recurrent precisely as in Figure 2 but this time for transitions to final states $2^+_f 1$ with E_x = 2.938 MeV and B(C2) = 12.1±7.1 e^2.fm^4, E_x = 7.082 MeV and B(C2) = 3.5±0.6 e^2.fm^4, E_x = 8.892 MeV and B(C2) = 4.8±1 e^2.fm^4, E_x = 10.838 MeV and B(C2) = 1.2 e^2.fm^4 and E_x = 10.990 MeV and B(C2) = 3.4±0.8 e^2.fm^4, respectively [45]. The left panel of these figures demonstrates that the ms calculation, which has a small contribution, fails to explain the measured data (open circles). It was apparent that the ms contribution largely underestimated the data at all considered momentum transfer. Considering the effect of cp as an enhancement to the ms calculation led to a strong revision to the form factors. It is very obvious that the cp effect significantly improved the outcome of the blue solid curve, but the data were still underestimated to some extent by this curve, where the blue solid curve was nearer to the data than that of the blue dashed curve of the ms effect. The calculations were reiterated in the middle panel of these figures just as in the left panel but now the effect of SRCs was included. The comparison among the C2 outcome without and with SRCs alongside those of the observed data was presented in the right panels. It is seen that including the effect of SRCs increased the strength of C2 result (red solid curve) and brought them in accordance with the data.
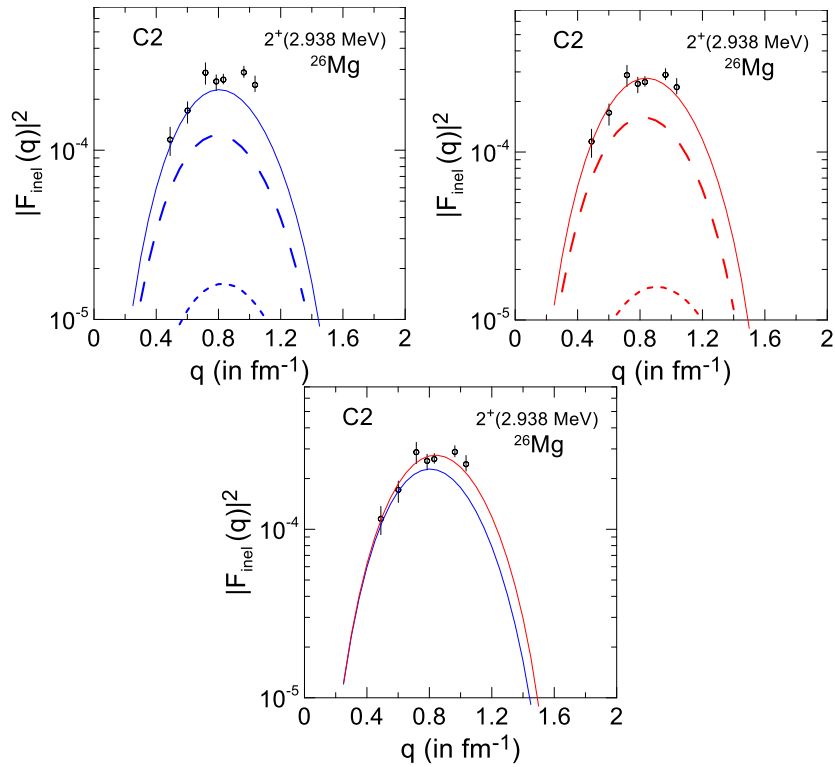
Figure 3: The same as in Figure 2 but for 2^+ (2.938 MeV) state.
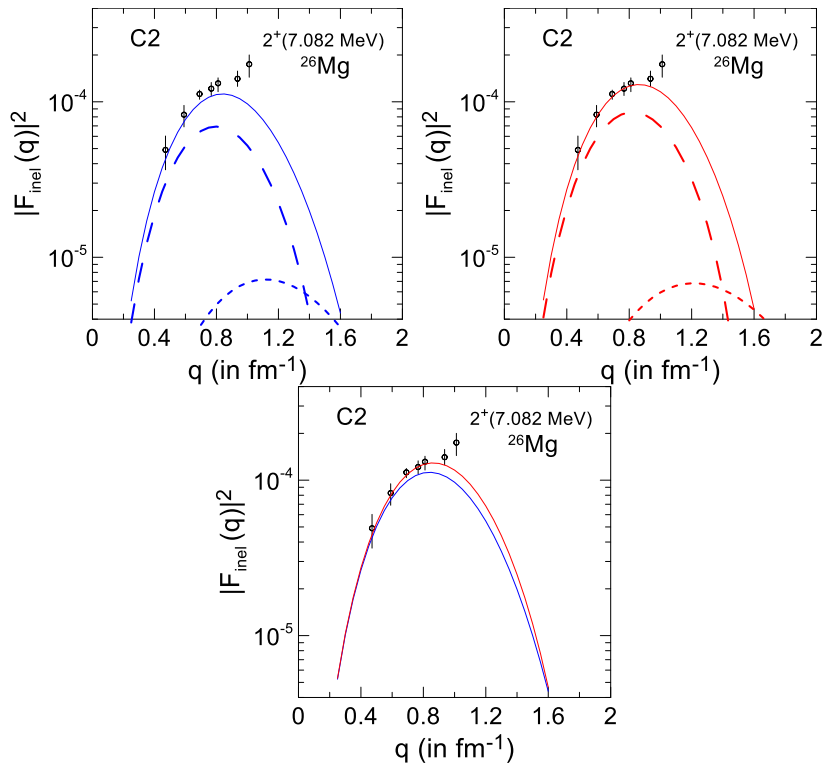
Figure 4: The same as in Figure 2 but for 2^+ (7.082 MeV) state.
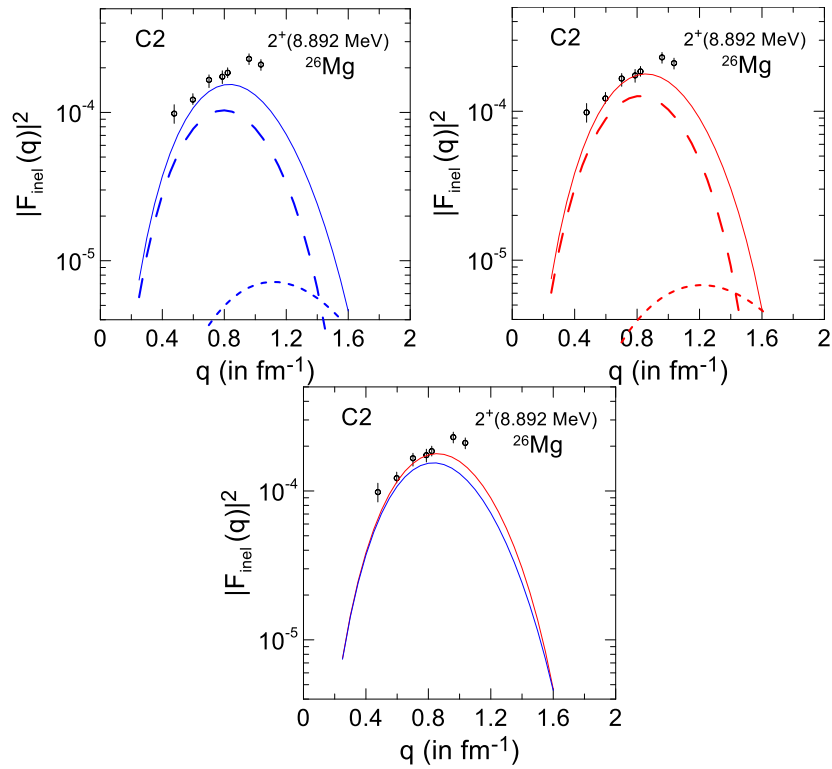
Figure 5: The same as5 in Figure 2 but for 2^+ (8.892 MeV) state.
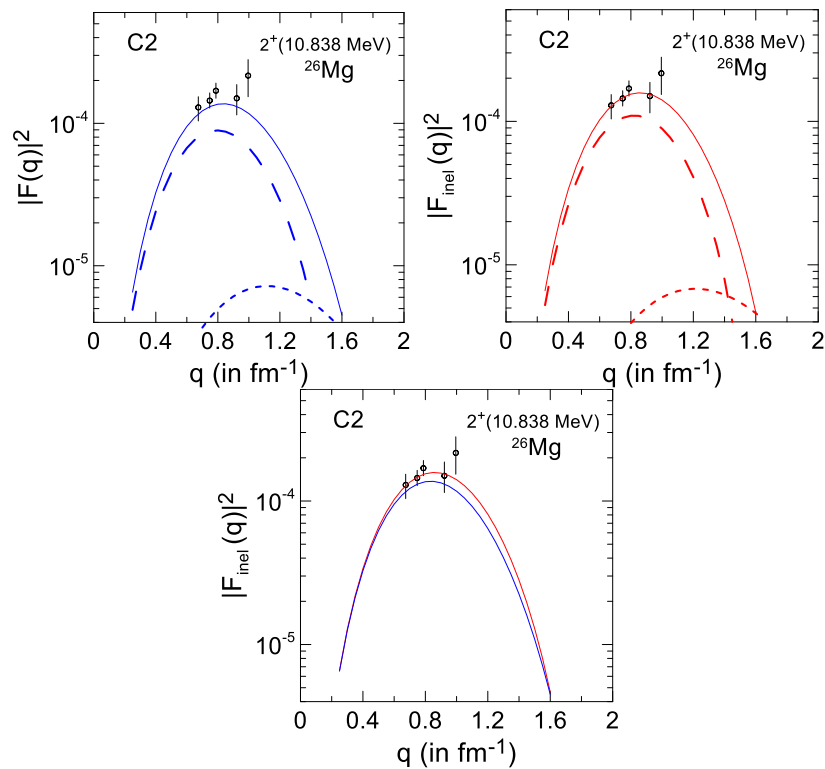
Figure 6: The same as in Figure 2 but for 2^+ (10.838 MeV) state.
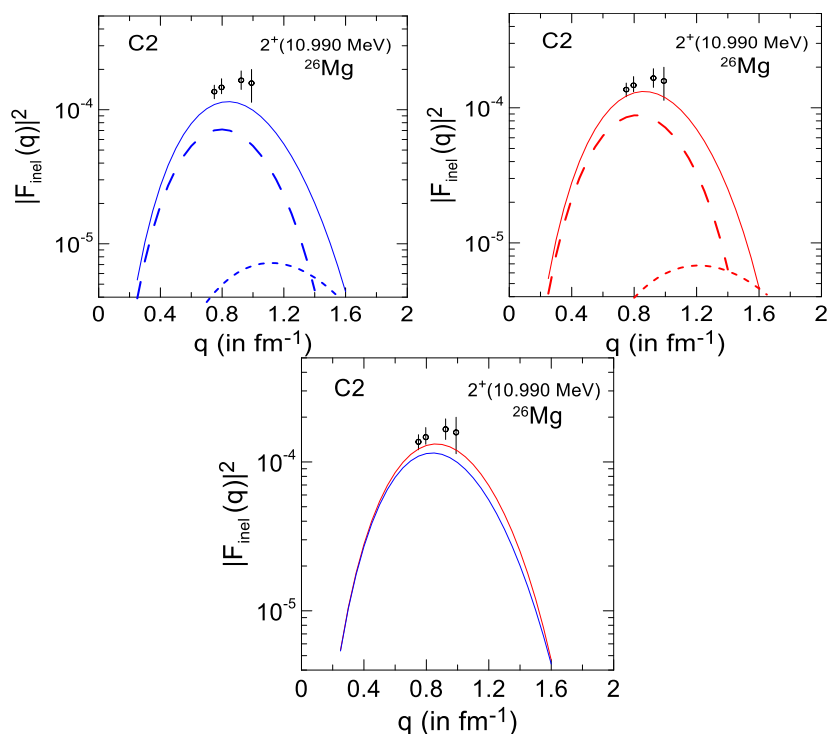
Figure 7: The same as in Figure 2 but for 2^+ (10.990 MeV) state.

In Figs. 8 to 11, the work as in Figure 2 was replicated but now for inelastic C3 form factors computed for transitions from the initial (ground) state 0^+1 to final states 3^-1 with ($E_x = 7.691$ MeV and B(C2) = 446 ± 223 e^2.fm^6), ($E_x = 7.830$ MeV and B(C2) = 546 ± 59 e^2.fm^6), ($E_x = 8.181$ MeV and B(C2) = 947 ± 154 e^2.fm^6) and ($E_x = 10.330$ MeV and B(C2) = 238 ± 115 e^2.fm^6), respectively [45]. It is clear that the parity of these transitions changed between the initial and final states.
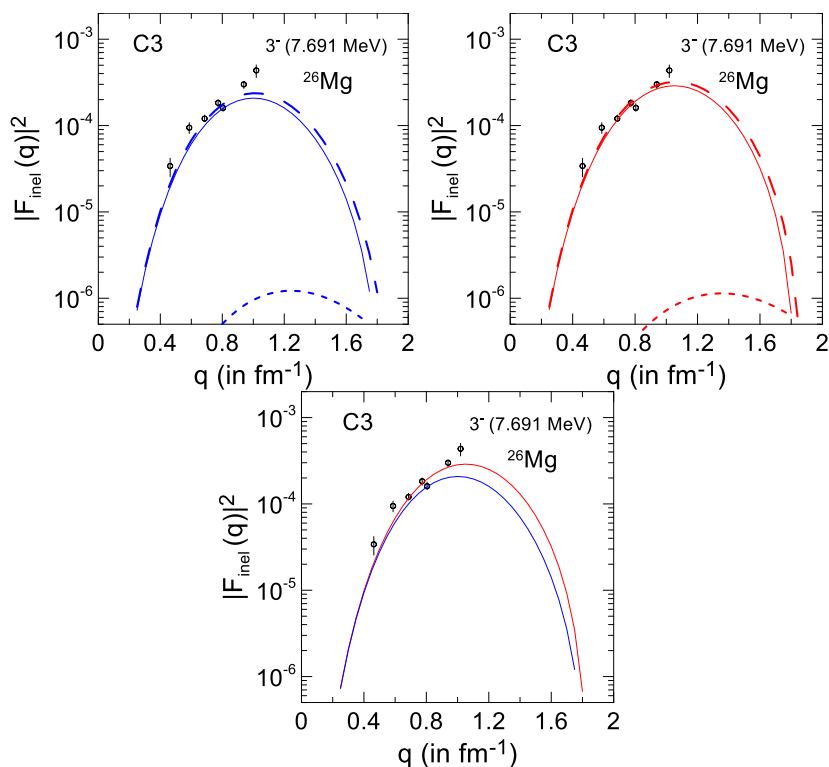
Figure 8: The same as in Figure 2 but for 3^- (7.691 MeV) state.
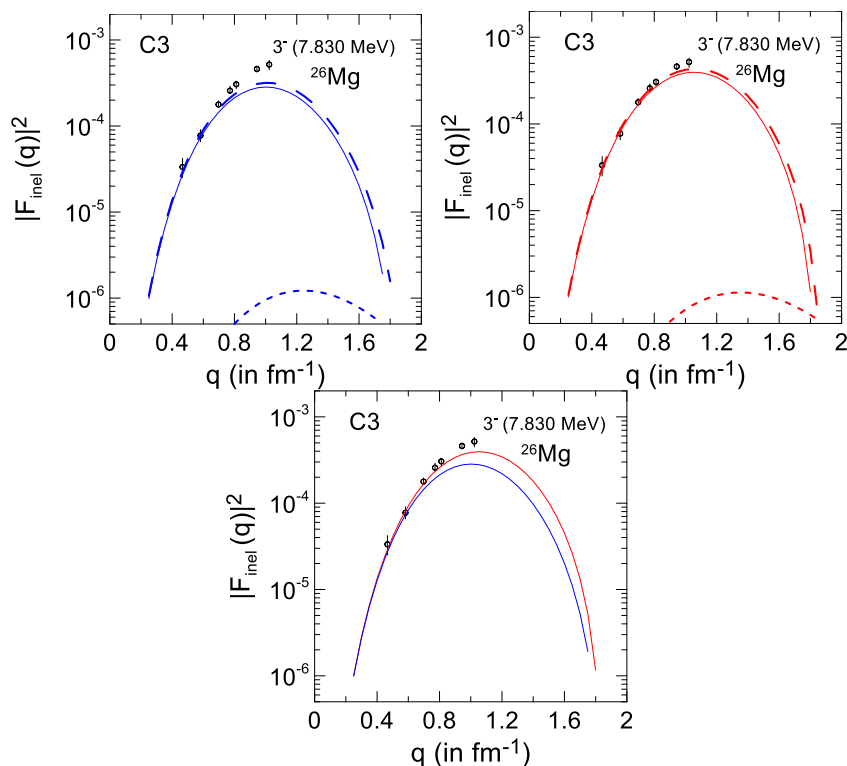
Figure 9: The same as in Figure 2 but for 3^- (7.830 MeV) state.
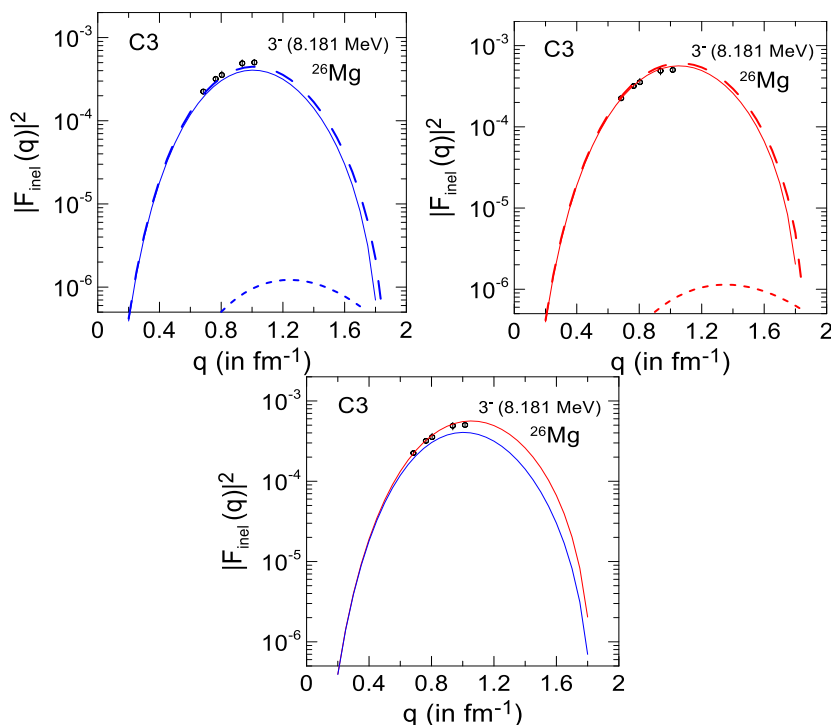
Figure 10: The same as in Figure 2 but for 3^- (8.181 MeV) state.

Figures 8 to 10 reveal that the ms involvement (dashed curve) in the left and middle panels is unsuccessful in clarifying the observed data (open circles). Where this involvement highly underestimated the data at all considered q values. The left and middle panels confirmed that the observed data were determined mainly through the cp effect (long-dashed curve), where the ms involvement is so small (of order 10^{-6}) compared to that of cp (of order 10^{-4}).

However, the cp effect shows the main role of transitions and form factors, as displayed in Figs. 8 to 10, where the cp effect of the blue long-dashed curve (without SRCs) slightly underestimated the data, while that of the red long-dashed curve (with SRCs) agreed well with the data. In the right panel of Figs. 8 to 10, the judgment amid the C3 form factors of the blue and red solid curves in conjunction with those of the data of open circles is exhibited. It is apparent that incorporating SRCs enhanced the C3 form factors (red solid curve) and made them consistent with the observed data.

Figure 11 indicates that the ms (dashed curve) and cp (long-dashed curve) effects (displayed in the left and middle panels) are essential in determining the C3 form factors, where both are in the same order of magnitude, but the cp effect is larger than that of the ms by about a factor of 2. The right panel of this figure showed the judgment amidst the inelastic C3 form factors of the blue and red solid curves in association with those of open circles. It was obvious that including the SRCs influence improved the C3 results (red solid curve) and led them to be in accordance with the measured data.
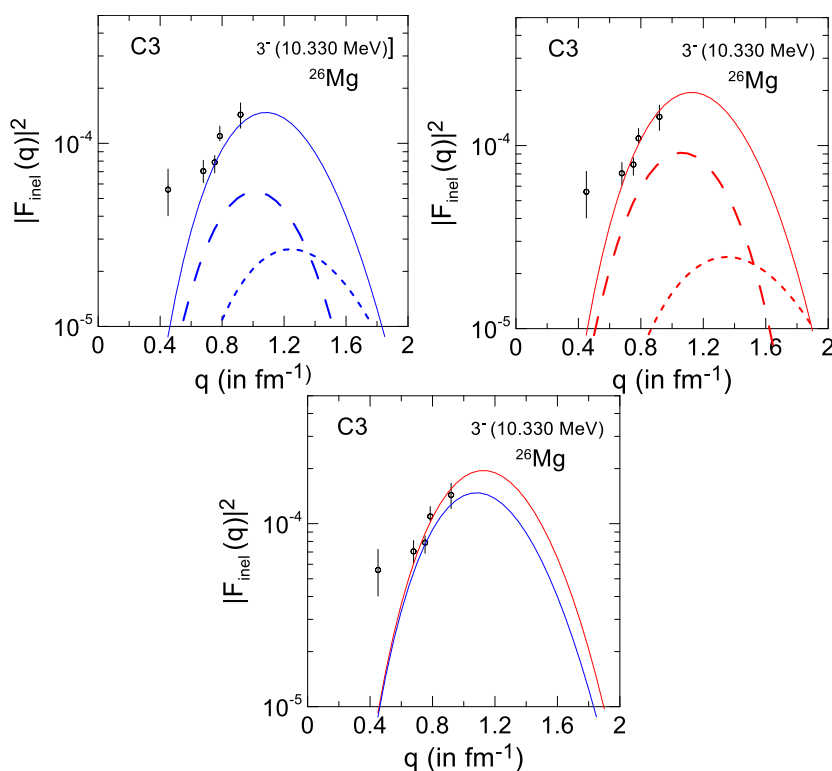
Figure 11: The same as in Figure 2 but for 3^- (10.330 MeV) state.

In Figs. 12 to 14, the calculations as in Figure 2 were restated, this time for inelastic C4 form factors calculated for transitions from the 0^+1 to the states 4^+1 with (E_x = 4.875 MeV and B(C2) = 26000 ± 7000 $e^2.fm^8$), (E_x = 5.720 MeV and B(C2) = 13000 ± 5000 $e^2.fm^8$) and (E_x = 10.680 MeV and B(C2) = $7400 + [^{+3700}_{=6700}$ $e^2.fm^8$), respectively [45]. Here, the parity of these transitions did not change between the initial and final states. These figures show that the ms participation (dashed curve) in the left and middle panels was unsuccessful in describing the data (open circles), where this participation evidently undervalued the data at considered q values. The left panel of these figures shows that the cp effect (blue long dashed curve) clearly overestimated the data in Figure 12, reasonably estimated the data in Figure 13, and clearly overestimated the data at $q < 0.8$ fm^{-1} in Figure 14. However, the cp effect, as a complement to the ms computation, provided a substantial change to the computed C4 form

factors (blue solid curve). It was noticed that the data in Figure 12 {Figure 13} were evidently {slightly} underestimated via the blue solid curve. While in Figure 14, the data were well estimated at $q \leq 1$ fm^{-1} and clearly underestimated at $1 < q < 1.15$ fm^{-1} by that curve. The computations were reiterated precisely in the middle panel of these figures as in the left panel, but here the SRC's effect was involved. In the right panel of these figures, the comparison among the C4 results (blue and red solid curves) in combination with those of the data is presented. It was seen that the addition of SRCs influence increased the improvement of C4 form factors (red solid curve) which made the computed outcome agrees with the data.
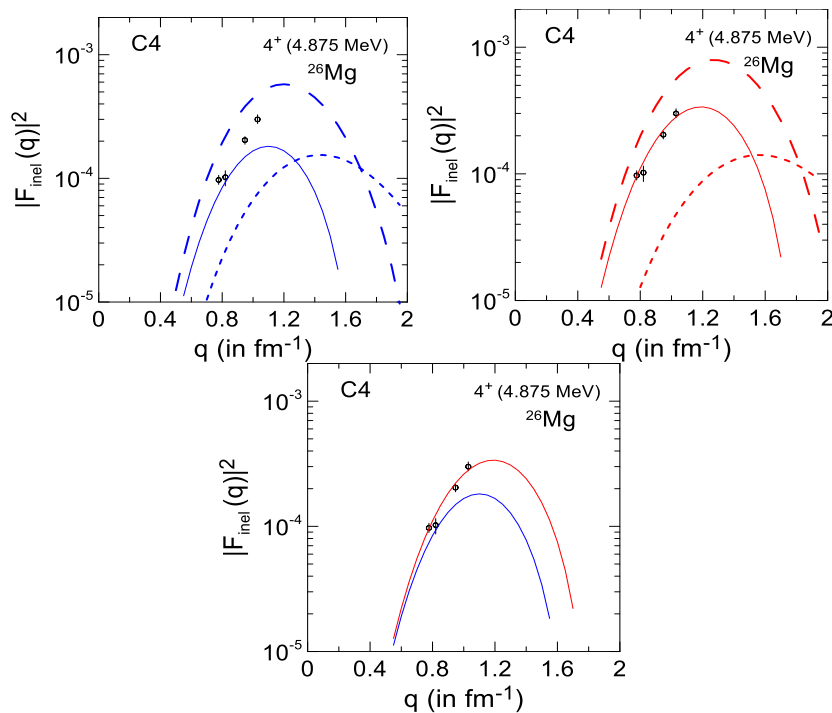
Figure -12: The same as in Figure 2 but for 4^+ (4.875 MeV) state.
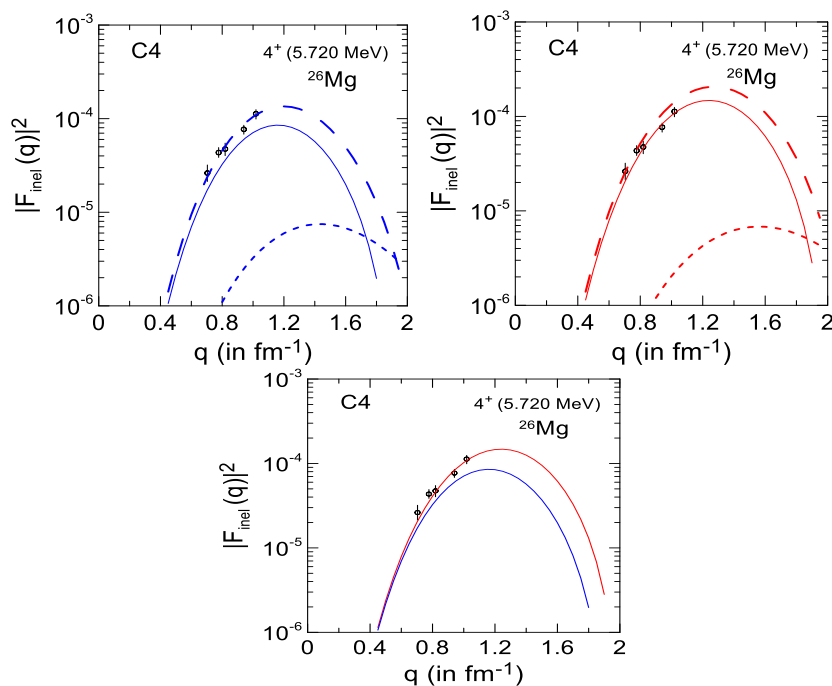
Figure 13: The same as in Figure 2 but for 4^+ (5.720 MeV) state.
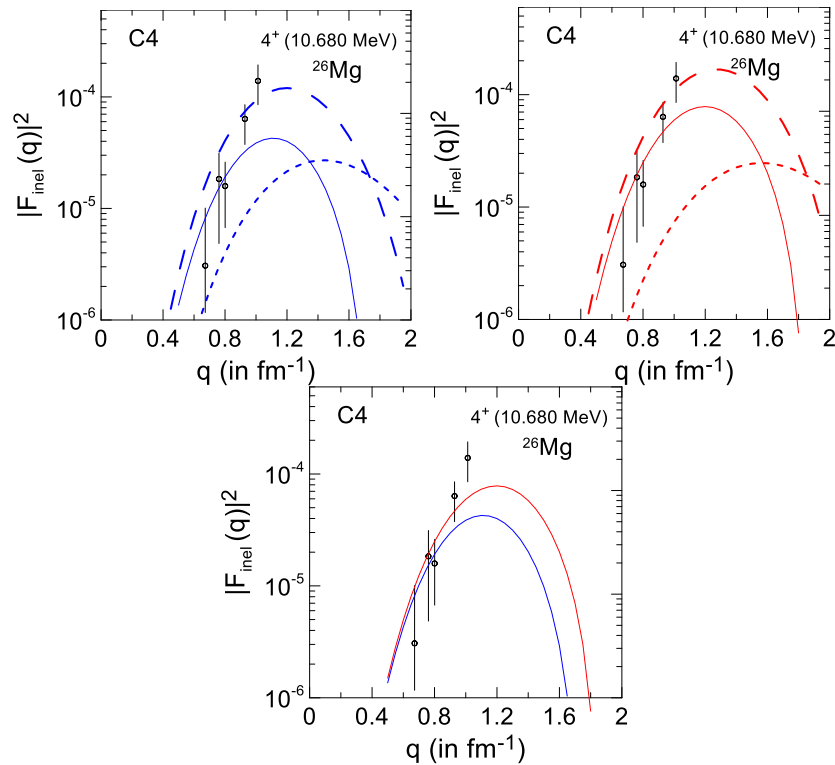
Figure 14: The same as in Figure 2 but for 4^+ (10.680 MeV) state.

4. Conclusions

It was found that considering the core polarization effect as an enhancement to the model space calculation greatly improved the computed form factors, but the data are still in disagreement to some extent. It was also found that there was a considerable predominance of short-range effects on the current computations, where inserting SRC's effects on inelastic form factors seemed to be fundamental for achieving a noticeable improvement in the calculated outcomes, which led to interpreting the measured data remarkably across the considered momentum transfers q.

Acknowledgment

References

[1]   R.Weiss, R.Cruz-Torres, N.Barnea, E.Piasetzky, O.Hen, "The nuclear contacts and short range correlations in nuclei," *Physics Letters B*, vol. 780, pp. 211–215, 2018.
[2]   O. Hen, B. A. Li, W.-J. Guo, L.B. Weinstein, E. Piasetzky, "Symmetry energy of nucleonic matter with tensor correlations," *Physical review C*, vol. 91, no. 2, pp. 25803-25815, 2015.
[3]   B.-J. Cai, B. A. Li, "Symmetry energy of cold nucleonic matter within a relativistic mean field model encapsulating effects of high-momentum nucleons induced by short-range correlations," *Physical Review C*, vol. 93, no. 1, pp. 14619-14633, 2016.
[4]   L.B. Weinstein, E. Piasetzky, D.W. Higinbotham, J. Gomez, O. Hen, R. Shneor, "Short range correlations and the EMC effect," *Physical Review Letters*, vol. 106, no. 5, pp. 52301-52306, 2011.
[5]   O. Hen, A. Accardi, W. Melnitchouk, E. Piasetzky, "Constraints on the large-x d/u ratio from electron-nucleus scattering at x> 1, " *Physical Review D*, vol. 84, no. 11, pp. 117501-117517, 2011.

[6] O. Hen, D.W. Higinbotham, G.A. Miller, E. Piasetzky, L.B. Weinstein, "The EMC effect and high momentum nucleons in nuclei," *Int. J. Mod. Phys. E*, vol. 22, no. 7, pp. 1330017-1330029, 2013.

[7] O. Hen, G.A. Miller, E. Piasetzky, L.B. Weinstein, "Nucleon-nucleon correlations, short-lived excitations, and the quarks within," *Rev. Mod. Phys.*, vol. 89, no. 4, pp. 45002-45015, 2017.

[8] O. Hen, E. Piasetzky, L.B. Weinstein, "New data strengthen the connection between short rangecorrelations and the EMC effect," *Phys. Rev. C*, vol. 85, no. 4, pp. 47301-47319, 2012.

[9] H. Gallagher, G. Garvey, G.P. Zeller, "Neutrino-nucleus interactions,"*Ann. Rev. Nucl. Part. Sci.*, vol. 61, pp. 355-378, 2011.

[10] L. Fields, J. Chvojka, L. Aliaga, O. Altinok, B. Baldin, A. Baumbaugh, A. Bodek, et al., "Measurement of muon antineutrino quasielastic scattering on a hydrocarbon target at E $\nu\sim$ 3.5 GeV," *Phys.Rev. lett.*, vol. 111, no. 2, pp. 22501-22506, 2013.

[11] G.A. Fiorentini, D.W. Schmitz, P.A. Rodrigues, L. Aliaga, O. Altinok, B. Baldin, A. Baumbaugh, et al., "Measurement of muon neutrino quasielastic scattering on a hydrocarbon target at E $\nu\sim$ 3.5 GeV," *Phys.Rev. lett.*, vol. 111, no. 2, pp. 22502-22511, 2013.

[12] R. Acciarri, C. Adams, J. Asaadi, B. Baller, T.Bolton, C. Bromberg, F. Cavanna, et al., "The detection of back-to-back proton pairs in charged-current neutrino interactions with the ArgoNeuT detector in the NuMI low energy beam line," *Phys. Rev. D*, vol. 90, pp. 12008-12021, 2014.

[13] L.B. Weinstein, O. Hen, E. Piasetzky, "Hammer events, neutrino energies and nucleon-nucleon correlations," *Phy. Rev. C*, vol. 94, no. 4, pp. 45501-45517, 2016.

[14] Altaf A Al-Rahmani and S F Kazem, "Elastic electron-nucleus scattering form factors of selected medium mass nuclei," *NeuroQuantology*, vol. 18, no. 8, pp.: 49-58, 2020.

[15] Altaf A. M. Al-Rahmani, "Study of the properties of Ru-isotopes using the proton-neutron interacting boson model (IBM-2)," *Baghdad Science Journal*, vol. 7, no. 1, pp. 76-89, 2010.

[16] R.B. Wiringa, R. Schiavilla, S.C. Pieper, J. Carlson, "Nucleon and nucleon-pair momentum distributions in A$\leq$ 12 nuclei," *Phys. Rev. C*, vol. 89, no. 2, pp. 24305-24321, 2014.

[17] J. Carlson, S. Gandolfi, F. Pederiva, S.C. Pieper, R. Schiavilla, K.E. Schmidt, R.B. Wiringa, "Quantum Monte Carlo methods for nuclear physics" *Reviews of Modern Physics*, vol. 87, no. 3, pp. 1067-1079, 2015.

[18] G. Hagen, A. Ekström,, C. Forssén, G. R. Jansen, W. Nazarewicz, et al., "Neutron and weak-charge distributions of the 48Ca nucleus," *Nat. Phys.*, vol. 12, no. 2, pp. 186–190, 2016.

[19] D. Lonardoni, A. Lovato, S.C. Pieper, R.B. Wiringa, "Variational calculation of the ground state of closed-shell nuclei up to A= 40," *Phys. Rev. C*, vol. 96, no.2, pp. 24326-24338, 2017.

[20] J. Ryckebusch, M. Vanhalst, W. Cosyn, "Stylized features of single-nucleon momentum distributions ," *Journal of Physics G, Nucl. Part. Phys.*, vol. 42, no. 5, pp. 55104-55123, 2015.

[21] M. Vanhalst, J. Ryckebusch, W. Cosyn, "Quantifying short-range correlations in nuclei,"*Phys. Rev. C*, vol. 86, no. 4, pp. 44619-44635, 2012.

[22] C. Colle, O. Hen, W. Cosyn, I. Korover, E. Piasetzky, J. Ryckebusch, L.B. Weinstein, "Extracting the mass dependence and quantum numbers of short-range correlated pairs from A (e, e′ p) and A (e, e′ p p) scattering," *Phys. Rev. C*, vol. 92, no. 2, pp. 24604-24618, 2015.

[23] S.E. Massen, H.P. Nassena and C.P. Panos, "A formula for the charge form factor of closed-shell nuclei and its application to ^{16}O," *J. Phys. G*, vol. 14, pp. 753-764, 1988.

[24] S.E. Massen and C.P. Panos, "An approximate treatment of the correlated charge form factor of light nuclei," *J. Phys. G: Nucl. Phys*, vol. 15, pp. 311-319, 1989.

[25] S.E. Massen," Correlated charge form factor and densities of the s-d shell nuclei," *J. Phys. G: Nucl.. Phys.* vol. 16, pp. 1713-1725, 1990.

[26] J.W. Clark and M.L. Ristig, "Cluster-Expansion Procedures for the Correlated Charge Form Factor,"*Nuovo Cimento A*, vol. 70, pp. 313-322, 1970.

[27] M.L. Ristig, W.J. Ter Low, J.W. Clark," Tensor Correlations in Nuclear Matter," *Phys. Rev. C*, vol. 3, pp. 1504-1513, 1971.

[28] W. Clark, "Variational theory of nuclear matter," *Prog. Part. Nucl. Phys.*, vol. 2, pp. 89-99, 1979.

[29] S.E. Massen and Ch. C. Moustakidis, "Systematic study of the effect of short range correlations on the form factors and densities of s-p and s-d shell nuclei," *Phys. Rev. C*, vol. 60, pp. 24005-24017, 1999.

[30] R. Jastrow, "Many-Body Problem with Strong Forces," *Phys. Rev.*, vol. 98, pp. 1479-1484, 1955.

[31] Adel K Hamoudi and Mahmoud A. Abbas, "Electron scattering from some even fp-and N50-shell nuclei with implanting the influence of short-range correlation functions," *Chinese Journal of Physics*, vol. 60, pp. 623-631, 2019.

[32] Adel K Hamoudi and Mahmoud A. Abbas," Electron scattering from some fp-shell nuclei with inclusion the effect of short-range correlation," *Iraqi Journal of Science*, vol. 61, no. 10, pp. 2540-2550, 2020.

[33] Adel K Hamoudi and Abdullah S. Mdekil, "The effect of short range correlation on the nuclear charge density distribution, elastic and inelastic electron scattering coulomb form factors of ^{18}O nucleus," *Iraqi Journal of Science*, vol. 56, no. 4A, pp. 2867-2879, 2015.

[34] F.I. Sharrad, A.K. Hamoudi, R.A. Radhi, Hewa Y. Abdullah, A.A. Okhunov and H. Abu Kassim, "Elastic Electron Scattering from Some Light Nuclei," *Chinese Journal of Physics*, vol. 51, pp. 452-465, 2013.

[35] Mahmoud A Abbas and Adel K Hamoudi," Elastic and inelastic C2 form factors of nickel isotopes and two-body correlations," *International Journal of Modern Physics E*, vol. 30, no. 10, pp. 2150080- 2150094, 2021.

[36] B.A. Brown, B.H. Wildenthal, C.F. Williamson, F.N. Rad, S. Kowalski, Hall Crannell, J.T. Brien,"Shell-model analysis of high-resolution data for elastic and inelastic electron scattering on ^{19}F," *Physical Reviews C*, vol. 32, pp. 1127–1156, 1985.

[37] P.J. Brussard and P.W.M. Glaudemans, *Shell-Model Applications in Nuclear Spectroscopy, North Holland, Amsterdam*, 1977, p. 14.

[38] T.W. Donnelly and I. Sick Rev., "Elastic magnetic electron scattering from nuclei," *Rev. Mod. Phys.*,vol. 56, pp. 461–566, 1984.

[39] B. A. Brown, R. Radhi and B.H. Wildenthal, "Electric quadrupole and hexadecupole nuclear excitations from the perspectives of electron scattering and modern shell-model theory," *Phys. Rep.*, vol. 101, pp. 313–358, 1983.

[40] L. J. Tassie, "A Model of Nuclear Shape Oscillations for E2 Transitions and Electron Excitation," *Austr. J. Phys.*, vol. 9, pp. 407-413, 1956.

[41] H. De Vries, C.W. De Jager, and C. De Vries, "Nuclear charge density distribution parameters from elastic electron scattering," *Atomic Data and Nuclear Data Tables*, vol. 36, pp. 495-536, 1987.

[42] G. Fricke, C. Bernhardt, K. Heilig, L. A. Schaller, L. Schellenberg, E. B. Shera, C. W. Dejager, "Nuclear ground state charge radii from electromagnetic interactions," *Atomic Dataand Nuclear Data Tables*, vol. 60, no. 2, pp. 177-285, 1995.

[43] B. H. Wildenthal, "Empirical strengths of spin operators in nuclei," *Prog. Part. Nucl. Phys.*, vol. 11, pp. 5-51, 1984.

[44] B. A. Brown, A. Etchegoyen, N. S. Godwin, W.D.M. Rae, W. A. Richter, W. E. Ormand, E. K. Warburton, J. S. Winfield, L. Zhao, C. H. Zimmerman, "Oxbash Code for Windows PC,MSU-NSCL report number 1289, 2005. For information on obtaining a copy contact the author at:brown@nscl.msu.edu.

[45] E. W. Lees, A. Johnston, S. W. Brain, C. S. Currant, W. A. Gillespie and R. P. Singhal,"The study of the excited states of ^{26}Mg below 11 MeV by inelastic electron scattering," *J. Phys. A: Math., Nucl. Gen.*, vol. 7, no. 8, pp. 936-974, 1974.